Efficient frequency doubling of a telecom 1560 nm laser in a waveguide and frequency stabilization to Rb D2 line

Yashuai Han (韩亚帅), Shanlong Guo (郭善龙), Jie Wang (王 杰),
Huifeng Liu (刘慧丰), Jun He (何 军), and Junmin Wang (王军民)[*]

State Key Laboratory of Quantum Optics and Quantum Optics Devices, Institute of
Opto-Electronics, Shanxi University, Taiyuan 030006, China
[*]Corresponding author: wwjjmm@sxu.edu.cn

We experimentally demonstrate efficient frequency doubling of a telecom 1560 nm distributed feedback diode laser with a 3 cm long MgO:PPLN waveguide with a conversion coefficient of 114%/W. We investigate optical inhomogeneities by measuring the quasi-phase-matching temperature curve. The ~2.7 mW of second-harmonic power at 780 nm is sufficient to detect the D_2 features using modulation transfer spectroscopy. The laser frequency is locked to a hyperfine transition of Rb D_2 line and typical residual frequency fluctuation of ±86 kHz (rms) is achieved within 30 min. Our experimental scheme can be used for realizing robust, compact, and highly accurate Rb stabilized 1560 nm laser systems for fiber-optic communication applications.

OCIS codes: 140.3515, 300.6420, 140.3425.

doi: 10.3788/COL201412.121401.

Optical frequency standards in optical communication bands have been needed for next-generation dense wavelength division multiplexing (DWDM) systems, optical fiber sensing, and high-accuracy measurement instruments such as wavelength meters and frequency synthesizers. Significant improvements have been made in optical frequency stabilized lasers by locking to transitions of acetylene $^{13}C_2H_2$[1–3]. However, detection of these sub-Doppler transitions requires high optical power, such systems usually involve a large optical standard gas cell in the Fabry–Perot cavity, which is complicated and hard to integrate.

A promising approach associated with frequency references near 1.5 μm is second-harmonic generation (SHG) of diode lasers and locking to narrow atomic sub-Doppler transitions or two-photon transitions of Rb, probed using the frequency-doubled light[4,5]. The quasi-phase-matching (QPM) waveguide is an attractive choice for SHG, which has the advantages of high efficiency, simplicity, and stability. Many techniques exist to obtain an error signal which can regulate the frequency of the laser. These techniques include saturation absorption spectroscopy (SAS), polarization spectroscopy (PS), frequency modulation spectroscopy[5], and modulation transfer spectroscopy (MTS)[6–9]. Compared with the other techniques, MTS has better signal-to-noise ratio (SNR) and completely no background, and it is less sensitive to the magnetic field, the fluctuation of laser intensity, and the temperature drift of atomic vapor cell, making it a good choice for frequency stabilization.

In this letter, a frequency-doubled 1560 nm distributed feedback (DFB) diode laser is locked to a Rb hyperfine transition using the MTS technique. We characterise the design and expect that the compact and robust Rb-stabilized 1560 nm laser system can be used as a calibrated reference for a separate laser wavelength meter, which would then be used to calibrate fiber telecom channels.

The experimental setup is shown in Fig. 1. We use a telecom 1560 nm fiber-pigtailed butterfly-sealed DFB diode laser (JDS Uniphase, 60 mW) as the laser source. An optical isolator is used to prevent optical feedback. The diode laser is driven by a low noise laser diode controller (Thorlabs LDC 205C) and a high-accuracy temperature controller (Thorlabs 200C). The 24 h drift of the current and the temperature are lower than 10 μA and 0.002 °C, respectively. The 1560 nm laser is coupled to a 3 cm long MgO:PPLN waveguide (HC Photonics).
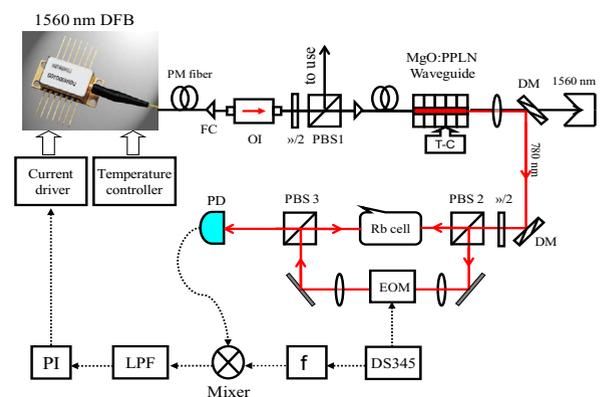
Fig. 1. Experimental setup. PM fiber, polarization-maintaining fiber; OI, optical isolator; FC, fiber coupler; DM, dichroic mirror; PD, photodiode; EOM, electro-optic modulator; LPF, low-pass filter; PI, proportional-integral controller; OSC, oscilloscope.

A rotatable polarization beam splitter (PBS 1) placed in front of the waveguide is used to obtain the correct polarization input. The waveguide is free-space output and the SHG beam is collimated by a lens. The SHG beam is separated from the non-converted transmitted fundamental wave (FW) beam through two dichroic mirrors.

The SHG beam is divided into two parts by a half-wave plate and PBS 2. The s and p polarization beams serve as the pump and probe lights, respectively. The two beams collinearly counter-propagate in a 5 cm long room temperature Rb vapor cell, which is magnet shielded with a μ-metal shielding. The pump beam is phase modulated by an electro-optic modulator (New Focus 4001-M). The interactions between the probe beam and the modulated pump beam within the Rb vapor transfer the modulation sidebands to the probe beam, via four-wave mixing. The sidebands generated in the probe field and the probe field itself create a beat frequency, detected on a photodiode. The generated signal is sent to a frequency mixer along with the local oscillator divided from the signal generator (DS 345).

The MTS signal output from the mixer goes into a proportional-integral (PI) controller after a 1.9 MHz low-pass filter. The phase of the reference signal supplied to the mixer is changed by altering the cable length between the local oscillator and the mixer. With the negative feedback to DFB laser driving current, we can lock the laser frequency to the hyperfine transition of Rb.

In order to measure the coupling efficiency into the waveguide, the temperature of the waveguide is detuned far from the QPM temperature, so that the attenuation of the FW beam by SHG can be neglected. With light originating from a single-mode fiber, a coupling efficiency of 80% is achieved corresponding to a maximum of 45 mW coupled to the waveguide.

The measured SHG power as a function of the waveguide temperature is shown in Fig. 2. The optimal measured QPM temperature is 43.0 °C. The observed asymmetric phase-matching temperature curve deviates from the theoretically predicted sinc^2 function (inset of Fig. 2). This situation might be caused by the optical inhomogeneities, especially the non-uniformity of the refractive

index along the pull axis in the growing process. Following the theoretical model in Ref. [10], we divide the waveguide along the pull axis into N regions with different refractive indexes n_i, lengths l_i, single-pass nonlinear conversion efficiencies η_i, and QPM temperatures T_P, and then the SHG power can be written as

$$P_{2\omega} = \sum_{i=1}^{N} \eta_i P_\omega^2 \frac{\sin^2(\Delta k_i l_i / 2)}{(\Delta k_i l_i / 2)^2} + 2 \sum_{i=1}^{N-1} \sum_{j=i+1}^{N} \sqrt{\eta_i \eta_j} P_\omega^2 \frac{\sin(\Delta k_i l_i / 2)}{(\Delta k_i l_i / 2)} \frac{\sin(\Delta k_j l_j / 2)}{(\Delta k_j l_j / 2)} \cos\left[\frac{(\Delta k_i l_i / 2)}{2} - \frac{(\Delta k_j l_j / 2)}{2}\right], \quad (1)$$

where $P_{2\omega} (P_\omega)$ is the SHG (FW) power and $\Delta k_{i,j}$ is the phase mismatch. Δk as a function of the crystal temperature T can be expanded in a Taylor series at the phase matching temperature T_P, with which the first order is

$$\Delta k = \frac{4\pi}{\lambda} \frac{\partial \Delta n}{\partial T} (T - T_P), \quad (2)$$

where $\Delta n = n_{2\omega} - n_\omega$. The experimental data are fitted well by the fitting Eq. (1) with $N = 4$ (Fig. 2).

For a lossless waveguide, the theoretically obtainable power P_{SHG} of the harmonic light field for perfect phase matching $\Delta k = 0$[11] is

$$P_{\text{SHG}} = P_{\text{coupled}} \tanh^2(\sqrt{\eta P_{\text{coupled}}}), \quad (3)$$

where $\eta = P_{\text{SHG}}/(P_{\text{coupled}})^2$ represents normalized conversion efficiency.

We neglect the propagation loss in the waveguide for both the FW and the SHG light and define the doubling efficiency as the 780 nm power at the end of the waveguide divided by the sum of the 780 and 1560 nm power at that point. The maximum achieved output power at 780 nm is 2.7 mW, converted from 45 mW FW beam within the waveguide. This corresponds to a conversion efficiency of 6%. Figure 3 presents the corresponding data. A theory curve following Eq. (3) with a normalized conversion efficiency $\eta = 114\%$/W reproduces the data. The transverse mode profile of SHG light in the inset of Fig. 3 shows a Gaussian distribution in both axes.

Fig. 2. SHG power as a function of the MgO:PPLN temperature with a FW field of 45 mW. Inset shows the sinc² curve.
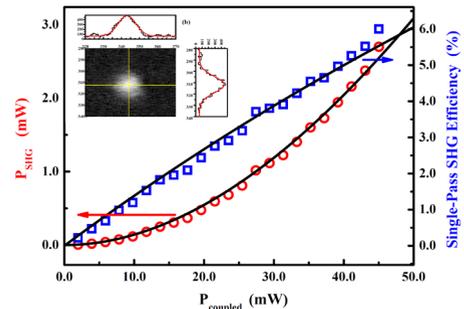
Fig. 3. SHG power and efficiency versus input FW power. Dots are the experimental data and the solid line is the fitting curve. Inset shows the transverse mode profile of SHG light.
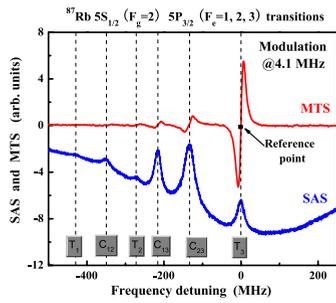
Fig. 4. SAS and corresponding MTS signals for ^{87}Rb $5S_{1/2}$ (F_{g}=2) →$5P_{3/2}$ (F_{e}=1, 2, 3) transitions.

Fig. 5. Allan standard variance of 1560 nm laser frequency as a function of measurement time. Inset shows the time race of the error signal while the laser is locked.

Scanning the 1560 nm DFB laser's injection current, we obtain the SAS signals and MTS signals of ^{87}Rb $5S_{1/2}$ ($F_{\mathrm{g}} = 2$) →$5P_{3/2}$ ($F_{\mathrm{e}} = 1, 2, 3$) transitions simultaneously (Fig. 4). The pump and probe beams are 150 and 70 μW, respectively. The modulation frequency is 4.1 MHz (0.67 times the natural linewidth) and the modulation index is 0.2. We choose the fixed modulation frequency as it gives the maximum signal gradients of the zero-crossing for MTS[7]. The MTS signals have good SNR ratio (28 with a 1.9 MHz detection bandwidth) and completely no background. The zero-crossings of the MTS signals are accurately centered on the corresponding atomic transition, and are not affected by magnetic field or wave plate angle-dependent shifts which upset SAS and PS. The stability of the lineshape is independent of changes in absorption due to fluctuations in polarization, temperature, and beam intensity. The strongest MTS signal is observed for the closed transition ($F_{\mathrm{g}} = 2$→$F_{\mathrm{e}} = 3$). Here four-wave mixing is an especially efficient process as atoms cannot relax into other ground states. This can be advantageous in the case where one wants to lock to closed transitions.

Taking the T_3 peak ($F_{\mathrm{g}} = 2$→$F_{\mathrm{e}} = 3$) of the MTS spectrum as the reference frequency, we lock the laser frequency to the zero-crossing point. The frequency stability is estimated using the slope of the zero-crossing point of the error signal. Figure 5 shows the frequency fluctuations of the DFB laser when the laser is locked using a PI controller to feed back on the current. The residual frequency fluctuation after being locked is ±86 kHz (rms) over 30 min of recording time (inset of Fig. 5). We used a series of measurements with different integration times to calculate the square root of the Allan variance (Fig. 5). We could find the frequency stability of stabilized 1560 nm laser is less than 1.5×10^{-11} for 250 s average time, which corresponds to frequency variations of 2.9 kHz at 1560 nm. It should be emphasized that the square root of Allan variance is derived from the error signal. For the next step, we hope to measure the Allan deviation from the beat note of a pair of Rb-stabilized DFB diode laser, which will more accurately reflect the optical frequency stability.

In conclusion, we demonstrate the SHG of telecom 1560 nm DFB diode laser in a 3 cm long MgO:PPLN
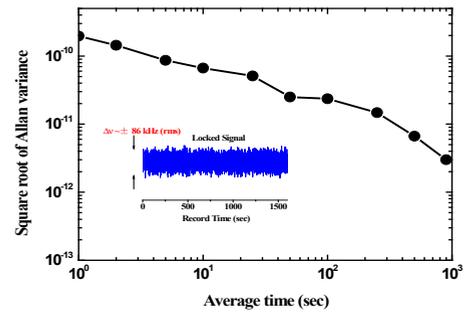
waveguide. We also investigate optical inhomogeneities by measuring the QPM temperature curve. This analysis can be a criterion to test the optical quality of doping crystals. Here 2.7 mW at 780 nm is generated with 45 mW of FW power coupled to the waveguide, corresponding to 6% conversion efficiency. We significantly improve the laser frequency stability after the frequency doubled laser is locked to ^{87}Rb $5S_{1/2}$ ($F_{\mathrm{e}} = 2$) →$5P_{3/2}$ ($F_{\mathrm{e}} = 3$) transition via MTS, compared with the free-running case. Combined with the MTS scheme, we expect that the compact and robust Rb stabilized telecom 1560 nm laser system can be used as a calibrated reference for a separate laser wavelength meter, which would then be used to calibrate fiber telecom channels.

References

1. P. Balling, M. Fischer, P. Kubina, and R. Holzwarth, Opt. Express **23**, 9196 (2005).
2. K. Nakagawa, Y. Sato, M. Musha, and K. Ueda, Appl. Phys. B **80**, 479 (2005).
3. V. Ahtee, M. Merimaa, and K. Nyholm, IEEE Trans. Instrum. Meas. **58**, 1211 (2009).
4. H. C. Chui, M. S. Ko, Y. W. Liu, T. Lin, J. T. Shy, S. Y. Shaw, R. V. Roussev, and M. M. Fejer, Opt. Lasers Eng. **44**, 479 (2006).
5. S. Masuda, A. Seki, and S. Niki, Appl. Opt. **46**, 4780 (2007).
6. J. Zhang, D. Wei, C. Xie, and K. Peng, Opt. Express **11**, 1338 (2003).
7. D. J. McCarron, S. A. King, and S. L. Cornish, Meas. Sci. Technol. **19**, 105601 (2008).
8. H. R. Noh, S. E. Park, L. Z. Li, J. D. Park, and C. H. Cho, Opt. Express **19**, 23444 (2011).
9. V. Negnevitsky and L. D. Turner, Opt. Express **21**, 3103 (2013).
10. H. Jiang, G. Li, and X. Xu, Opt. Express **17**, 16073 (2009).
11. K. R. Parameswaran, J. R. Kurz, R. V. Roussev, and M. M. Fejer, Opt. Lett. **27**, 43 (2002).